Heliyon 10 (2024) e39910

Contents lists available at ScienceDirect

Heliyon

journal homepage: www.cell.com/heliyon

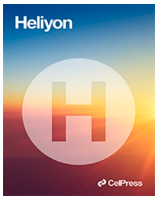

Research article

A density functional theory study of a series of symmetric dibenzylideneacetone analogues as potential chemical UV-filters

Buhari Magaji [a,1], Parvesh Singh [a], Adam A. Skelton [b], Bice S. Martincigh [a,*]

[a] School of Chemistry and Physics, University of KwaZulu-Natal, Westville Campus, Private Bag X54001, Durban, 4000, South Africa
[b] School of Pharmacy and Pharmacology, University of KwaZulu-Natal, Westville Campus, Private Bag X54001, Durban, 4001, South Africa

ARTICLE INFO

Keywords:
DFT
TD-DFT
NMR
UV
IR
GIAO
α,β-unsaturated ketones

ABSTRACT

The aim of this research was to provide valuable insights on symmetrical α,β-unsaturated ketones as potential chemical ultraviolet (UV) filters from experimental data and theoretical aspects. Towards this end, density functional theory (DFT/B3LYP) calculations on a series of symmetrical α,β-unsaturated ketones, (*1E,4E*)-1,5-bis[4-(R)phenyl]penta-1,4-diene-3-one (R = methylthio, **1**; R = dimethylamino, **2**; R = ethyl, **3**), were performed to determine the effect of different electron-donating substituents on their stability when exposed to solar UV radiation. Their molecular structures, and UV–visible, infrared (IR) and NMR (^{1}H and ^{13}C) spectra were theoretically obtained from their optimized geometries with the B3LYP/6–311++ G (d, p) basis set and were compared with the experimental results. Conformational analysis was performed and the most stable conformer of each compound was identified as the *trans-trans* conformer, which was further supported by experimental NMR data. The UV spectra and effect of solvent polarity and proticity were studied by the time-dependent-DFT (TD-DFT) approach with the B3LYP/6–311++G (d, p) level of theory. Furthermore, various molecular parameters like dipole moment, frontier molecular orbital (FMO) energies, $\Delta E_{HOMO\text{-}LUMO}$ gap, lifetime of the first excited state (τ), global chemical reactivity descriptors, and natural bond orbital analysis were predicted at the same level of theory and compared with the experimental data. Inspection of the active FMOs revealed the photoinstability trends of **1** and **3** under UV irradiation. However, introducing a -N$(CH_3)_2$ substituent to **2** at the *para*-position improves its photostability towards simulated solar UV radiation. Thus, compound **2** has the potential to provide efficient broad-spectrum protection against UV radiation. This work has shown that molecular modelling strategies can assist to rationalize experimental findings and also support the identification of photoproducts of **1** and **3**.

1. Introduction

Solar ultraviolet (UV) radiation can be harmful to humans, damaging both the skin surface and inner structure of the skin. The solar UV radiation which reaches the earth's surface is a combination of ultraviolet B (UVB, ranging from 290 to 315 nm) and ultraviolet A (UVA, ranging from 315 to 400 nm). Overexposure to UV radiation can cause sunburn [1,2], skin wrinkles [3–5], erythema [5,6], inflammation [7,8], and skin cancer [1,9–11]. Photoprotection against harmful UV radiation can be achieved by staying out of the sun

* Corresponding author.
E-mail address: martinci@ukzn.ac.za (B.S. Martincigh).
[1] Present address: Department of Chemistry, Gombe State University, P.M.B. 127, T/Wada, Gombe, Nigeria.

https://doi.org/10.1016/j.heliyon.2024.e39910
Received 19 June 2024; Received in revised form 24 October 2024; Accepted 27 October 2024
Available online 29 October 2024

during the peak hours of the day, proper dressing, and use of sunscreens [1,6].

Sunscreens are photochemical systems containing chemical UV-filters and physical absorbers, that can play a major role in skin cancer prevention and sun protection [12–15]. Consequently, their use has increased markedly with the increasing incidence of skin cancer and photoaging effects caused by UV radiation. Of interest to this research are chemical UV-filters. Many sunscreen chemical filters absorbing in the UVA or/and UVB range are in use, but their safety and efficacy are still in question [16,17]. In response to the growing awareness of the deleterious effects of UV light [18], and lack of photostability of some of the available chemical UV-filters [19], a series of novel symmetrical α,β-unsaturated ketones were synthesized by means of an improved Knoevenagel condensation method and their photostability was explored in various solvents of different polarity and proticity [20].

Symmetrical α,β-unsaturated ketones have attracted much attention in the scientific community in the past decades due to their broad range of pharmaceutical applications and biological activities [21–26], but little or no attention has been given to their photostability towards UV radiation. The presence of the pentadiene-3-one moiety and a complete delocalized π-electron system on their two phenyl rings make them biologically active. This unique structure has given them the ability to absorb UV radiation. The aim of this study was to assess from a theoretical and experimental perspective the effect of solvent polarity and different electron-releasing substituents on the stability of (1*E*,4*E*)-1,5-bis[4-(methylthio)phenyl]penta-1,4-dien-3-one, **1**; (1*E*,4*E*)-1,5-bis[4-(dimethylamino) phenyl]penta-1,4-dien-3-one, **2** and (1*E*,4*E*)-1,5-bis[4-(ethyl)phenyl]penta-1,4-dien-3-one, **3** (see Fig. 1 for structures) and to see if they could find application in sunscreen formulations as new chemical UV-filters.

Density functional theory (DFT) and the B3LYP functional have been shown to be exceptionally effective in describing structural, spectral, and various other properties of important chemical and biological molecules, due to their low computational cost, high accuracy, and popularity in quantum chemistry. The DFT/B3LYP/6–311++G (d, p) level of theory was used in this work to obtain

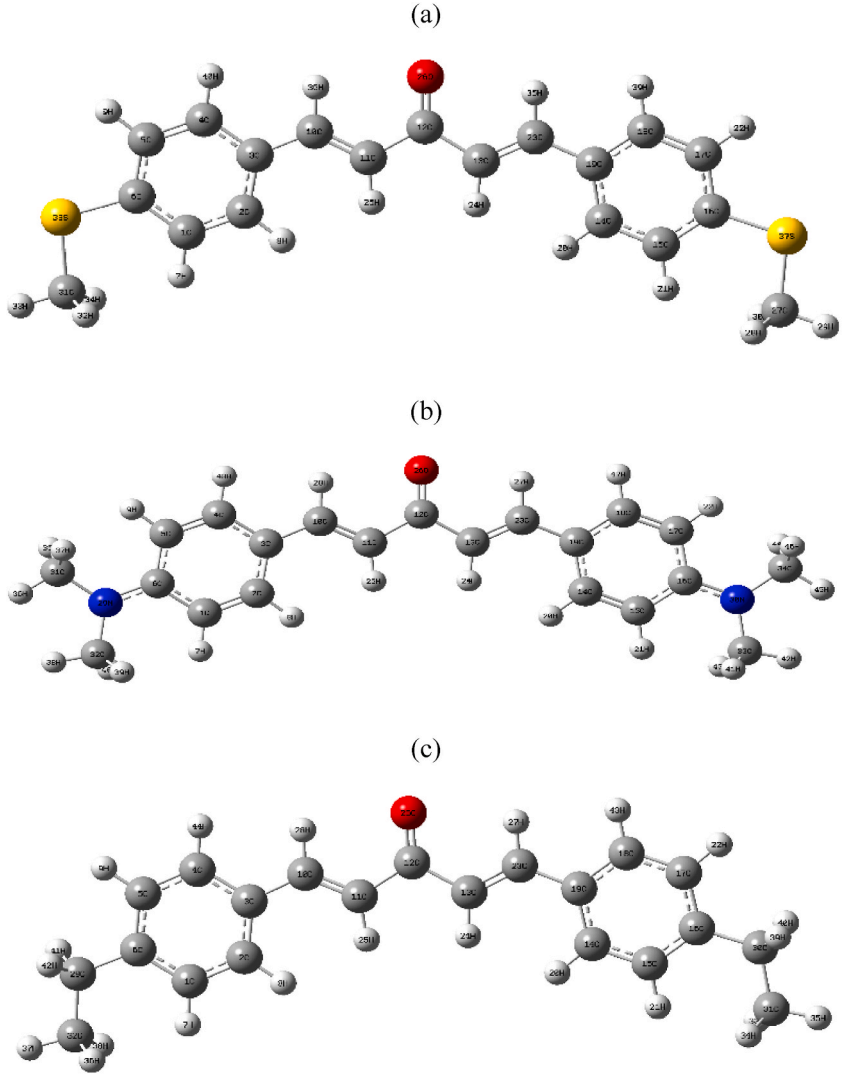

Fig. 1. Optimized geometries of (a) **1**, (b) **2**, and (c) **3** obtained by using the DFT/B3LYP method with the 6-311G++ (d, p) basis set.

complementary information to that gleaned in our experimental study [20] that would enhance our understanding of the behaviour of the studied molecules. To this end, computational studies provided an in-depth insight into the vibrational and spectroscopic properties, the lifetime of the first excited state (τ), frontier molecular orbitals, and effect of solvent polarity on the stability of the present compounds. More so, nuclear magnetic resonance (NMR) spectra and various other molecular properties like dipole moment, global chemical reactivity, and natural bond orbital (NBO) were included for a better understanding of molecular properties. We believe that the effort made towards discovery of new chemical UV filters in this work is unique, and to date has not been previously reported.

2. Methodology

2.1. Synthesis and characterisation

The target compounds were synthesized and characterised as described in our previous report [20].

2.2. Computational details

Initially, the stable conformer and energy minima of each compound were determined. All calculations were performed with Gaussian 09W [27]. The ground state geometries and conformations of **1**–**3** were computed by using DFT with the B3LYP functional and the 6–311++G (d, p) basis set. B3LYP is the most common among DFT models. It is a hybrid method by Becke [28] and Lee et al. [29]. The model uses exact exchange and gradient corrected density functional approximations to calculate correlation energies from electron densities [30–32]. B3LYP has been embraced to give relatively good geometries of most organic and organometallic compounds [33,34]. Hence, this method was used. There are some criticisms noted such as poor estimation of barrier heights and weak interactions [35,36]. Furthermore, for a better computational output, a larger basis set is required since approximations of the orbitals are obtained by imposing less restriction on the location of electrons in space. In this work, Becke's three parameter hybrid exchange DFT functional together with Lee, Yang and Parr's correlation functional (B3LYP) [28,29] was coupled with the 6–311++G (d, p) basis set. An update on basis sets was published by Jensen [36] and Hill [37].

The harmonic frequency calculation was performed at each optimized geometry. The present optimized geometry corresponds to the minimum energy on the potential energy surface as real values of IR frequencies were obtained. Some of the important fundamental bands that appeared in the IR spectra of **1**–**3** were assigned by using animated modes with the help of Gauss View 5.0.8 [38]. We have scaled the vibrational frequency numbers with a standard scaling factor of 0.967 because the DFT-calculated harmonic vibrational frequencies are usually larger than those observed experimentally [39,40]. The theoretical electronic absorption spectra have been calculated by using the time-dependent DFT (TD-DFT) method [41,42]. The values of excitation energies (E), oscillator strength (*f*), wavelengths (λ), and energy gaps ($\Delta E_{HOMO\text{-}LUMO}$) for the molecules have been calculated in vacuum and in different solvents of varying polarity and proticity. The Integral Equation Formalism Polarized Continuum Model (IEF-PCM) was used to study the effect of solvent polarity [43,44]. Three solvents were used in the present study: ethyl acetate ($\varepsilon = 6.02$), methanol ($\varepsilon = 32.7$), and DMSO ($\varepsilon = 46.7$). The gauge independent atomic orbital (GIAO) approach within the DFT method is most reliable for calculating NMR spectra [45–47]. The ^{1}H and ^{13}C NMR chemical shifts for **1**–**3** were computed at the GIAO-B3LYP/6–311++G (d, p) level of theory in chloroform ($CHCl_3$) by using the PCM model. The chemical shifts were calculated relative to tetramethylsilane (as reference). The position of the localization of electron populations has been shown through the calculated electronic populations of the highest occupied molecular orbital (HOMO) and lowest unoccupied molecular orbital (LUMO) with their energies. Other electronic properties such as ionization potential (IP), electron affinity (E_A), global hardness (η), and global softness (S), were calculated from Equations (1)–(4) [48–53].

The ionization potential (IP) and electron affinity (E_A) were calculated from Equations (1) and (2) respectively:

$$IP = E_c - E_n \tag{1}$$

$$E_A = E_a - E_n \tag{2}$$

where E_c, E_a and E_n are the cationic energy (+1 charge), anionic energy (−1 charge) and neutral energy (0 charge) respectively, whereas the chemical hardness and softness were obtained from Equations (3) and (4) respectively:

$$\eta = \frac{IP - E_A}{2} \tag{3}$$

$$S = \frac{1}{2\eta} \tag{4}$$

Charge transfer is one of the essential factors for understanding the stability of a molecule. This was investigated from natural bond orbital (NBO) analysis [54] by monitoring the atom charges [55]. The natural atomic charge (NAC) plays an important role in applying quantum mechanical calculations to molecular systems, as the atomic charge affects the electronic structure, dipole moment, and other properties of the molecule [56]. Effects of electron-donating and withdrawing groups (EDG and EWG) were investigated to gain insights on the stability of the present compounds.

3. Results and discussion

In line with the research interest, DFT calculations were performed on compounds **1**–**3** to obtain more insight on their electronic and geometrical properties, and to predict their photodegradation trend when exposed to simulated solar radiation. These results were compared with our experimental findings [20]. Inspection of the active frontier molecular orbitals (FMOs) revealed the photo-instability trends of compounds **1** and **3** under UV radiation with the formation of photoproducts ((*E*)-1,5-bis(4-(methylthio)phenyl) pent-1-en-3-one and *(E)*-1,5-bis(4-(ethyl)phenyl)pent-1-en-3-one for compounds **1** and **3** respectively). Interestingly, compound **2** was observed to be considerably more photostable towards simulated UV radiation. These findings, agree with our previously reported experimental results [20]. Thus, this work has shown that molecular modelling strategies can assist to rationalize experimental findings.

3.1. Conformational analysis

In order to investigate the possible conformers of **1**–**3**, different conformations were explored by changing the orientation of the two aromatic rings attached to the chromophoric (pentadiene-3-onyl) moiety as shown in Supplementary Material Figs. S1–S3. Potential energy scans were performed on the different conformational possibilities (*trans-trans*, *cis-cis*, *cis-trans* and *trans-cis*) of the compounds, at the B3LYP/6–311++G (d, p) level of theory. The conformation with the lowest energy was considered as the reference to calculate the relative energy, $\Delta E_{relative}$, for all the compounds. The energy differences ($\Delta E_{relative}$) between the conformers (*trans-trans*, *cis-trans*, *trans-cis* and *cis-cis*) are given in Table 1. The energy difference for the lowest energy conformer (*trans-trans*) is lower than kT (2.478 kJ mol^{-1} at room temperature), thereby suggesting that the *trans-trans* conformer may exist at room temperature. The energy differences for the other conformers (*cis-trans*, *trans-cis* and *cis-cis*) are much larger than kT, indicating their non-existence at room temperature. These results were in good agreement with the experimental NMR data. Thus, the rest of the study was based only on the *trans-trans* conformers for all the compounds (**1**–**3**).

3.2. Optimized molecular geometry analysis

The optimized molecular structures of **1**–**3** and their hydrogenated photoproducts obtained by using the DFT/B3LYP method with the 6-311G++ (d, p) basis set are presented in Fig. 1 and Supplementary Material Fig. S4 for comparison. Since a crystal structure of compound **1** could be obtained, it was possible to compare the optimized geometric parameters (bond lengths, bond angles and torsion angles) of compound **1** with the structural parameters obtained from the crystallographic information file (CIF). (CCDC 2261682 contains the supplementary crystallographic data for compound **1**. These data can be obtained free of charge from the Cambridge Crystallographic Data Centre via www.ccdc.cam.ac.uk/structures.) Some selected results are presented in Table 2. Compound 1 possesses a C1 point group. The pentadiene-3-onyl chromophoric moiety (C9-C10-C11-O1) attached to the two methylthio substituted phenyl rings (C8-C5-C6 and C12-C13-C18) subtend dihedral angles that are essentially the same (34.7102(6)°) and, hence, the non-planarity of the methylthio substituted phenyl rings with respect to the chromophoric moiety of the compound (Fig. 1). Generally, the optimized structural parameters were found to be in the normal range and were found to be in good agreement with the XRD data (R^2 = 0.9995 and 0.9997 for bond lengths and angles respectively). However, it is observed that some of the bond lengths and angles are slightly overestimated, while a few are underestimated. These discrepancies may be due to the fact that the theoretical calculations correspond to isolated molecules in the gaseous phase and the experimental results belong to molecules in the solid state. The geometry of solid-state structures is subject to intermolecular forces, such as van der Waals interactions and crystal packing forces, which make most of the experimental bond lengths to be shorter than the theoretical ones. The optimized molecular geometry obtained by the B3LYP/6-311G++ (d, p) method and XRD were overlaid (Fig. 2) and the root mean square deviation (RMSD) and maximum deviation (MAD) values were found to be 0.5900 Å and 1.1382 Å respectively. Furthermore, the conformation of the molecular structure obtained by XRD appears to be a concave geometry as opposed the theoretical optimized structure as shown in Fig. 1.

3.3. Vibrational analysis

The infrared vibrational frequencies of the most stable conformers of **1**–**3** were calculated with the DFT B3LYP/6–311++G (d, p) method. In general, harmonic IR frequencies overestimate the corresponding experimental frequencies due to systematic errors caused by basis set incompleteness, neglect of vibrational anharmonicity, and various approximations used in the present DFT calculations. Therefore, a uniform scaling factor of 0.967 was used to scale down the harmonic frequencies for achieving good correlation with the experimental frequencies [40]. Vibrational mode assignments were made by visual inspection of the modes animated by the Gauss

Table 1
Relative energies of the different conformers of **1**–**3** presented in Supplementary Material Figs. S1–S3.

Compound	Relative energy/kJ mol^{-1}			
	trans-trans	*cis-cis*	*cis-trans*	*trans-cis*
1	0	38	17	17
2	0	38	17	17
3	0	42	21	21

Table 2
Comparison of selected optimized structural parameters for **1** with corresponding XRD data. XRD data are from Ref. [20]. Atom numbering corresponds with Fig. 1 in Ref. [20].

Parameter	XRD	B3LYP/6-311G ++(d, p)
Bond distance/Å		
S2-C19	1.798(2)	1.821
S2-C16	1.764(4)	1.775
S1-C2	1.759(2)	1.775
S1-C1	1.801(2)	1.821
O1-C10	1.230(3)	1.228
C8-C5	1.460(3)	1.457
C13-C12	1.460(3)	1.457
Bond angle/°		
C16-S2-C19	102.46(10)	103.87
C2-S1-C1	102.81(11)	103.75
O1-C10-C11	122.40(2)	122.15
01-C10-C9	122.30(2)	122.13
C11-C10-C9	115.30(2)	115.72
Torsion angle/°		
C19-S2-C16-C17	158.20(3)	−179.99
C1-S1-C2-C7	−3.79(7)	0.01
Dihedral angle/°		
C9-C10-C11-O1	32.29	0
C8-C5-C6	34.71(5)	0
C12-C13-C18	34.71(6)	0

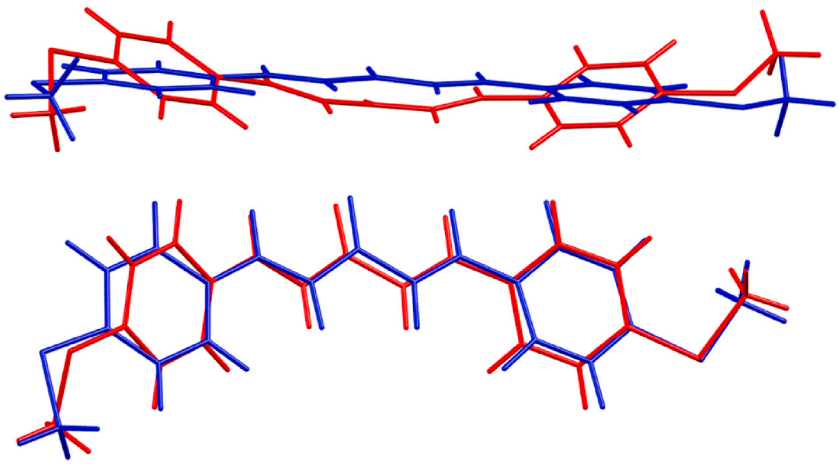

Fig. 2. Molecular overlays of the optimized theoretical structure (blue) and that obtained by XRD (red) for **1**. (For interpretation of the references to colour in this figure legend, the reader is referred to the Web version of this article.)

View program [38]. Selected calculated vibrational frequencies are compared with the experimental vibrational frequencies in Table 3. All the assignments given in Table 3 were determined from reported IR frequencies [57]. A comparison between the experimental and predicted IR spectra of the titled compounds is presented in Fig. 3 and Supplementary Material Figs. S5 and S6. The

Table 3
Some experimental and DFT-computed IR frequencies for compounds **1**–**3**.

Compound Code		IR frequency/cm^{-1}					
		C=O	C=C$_s$	C=C$_{ar}$	C-S	C-N	C_2H_5
1	Exp.[a]	1645	1617	1586	815	–	–
	DFT	1649	1630	1598	820	–	–
2	Exp.[a]	1684	1630	1548	–	1159	–
	DFT	1641	1636	1600	–	1186	–
3	Exp.[a]	1645	1622	1588	–	–	2965
	DFT	1652	1634	1592			2965

s - stretch and ar - aromatic.
[a] Experimental data are from reference [20].

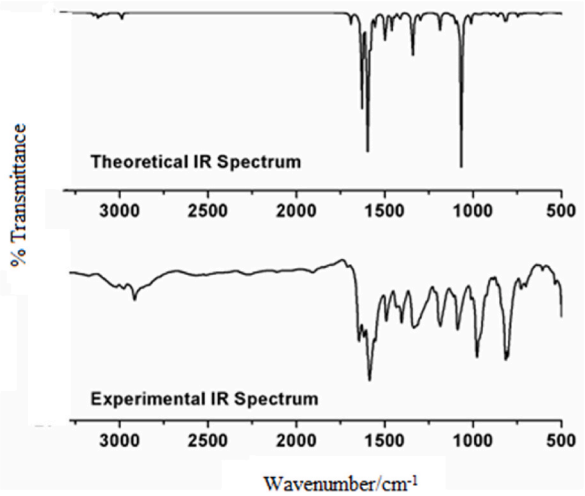

Fig. 3. Theoretical and experimental IR spectra of **1**.

scaled infrared vibrational frequencies showed good agreement with the experimental data. The correlation between the calculated and the experimental vibrational frequencies is shown in Supplementary Material Fig. S7. As can be seen from this figure, a good correlation was obtained between the calculated and experimental vibrational frequencies with high correlation coefficients.

3.3.1. C-H vibrations

The C-H stretching vibration in alkenes and aromatic structures occurs between 2850 and 3100 cm^{-1} and 3000 - 3100 cm^{-1} respectively [57–59]. The experimental IR band for the C-H stretching vibrations of **1** are observed at 2916 and 3017 cm^{-1} while the calculated C-H stretching vibrations appeared at 2914 and 3031 cm^{-1}. For **2**, the experimental C-H stretching vibrations are observed at 2891 and 3012 cm^{-1} with the computed C-H stretching vibrations at 3002 and 3072 cm^{-1} respectively. The experimental C-H stretching vibrations of **3** are observed at 2932 and 3026 cm^{-1} with calculated C-H stretching vibrations appearing at 2959 and 3040 cm^{-1}. The characteristic IR band due to the C-H aromatic vibration of **1**–**3** appears in the region 3012 - 3026 cm^{-1}. The predicted scaled frequencies corresponding to these vibrations were found close to the experimental ones in the region 3031 - 3072 cm^{-1}.

3.3.2. C-S, C-N and C_2H_5 vibrations

The S-CH_3, C-N and C_2H_5 stretches are expected in the regions 600 - 850 cm^{-1}, 1080 - 1360 cm^{-1} and 2652 - 2972 cm^{-1} respectively [59,60]. The C-S bond is highly polarizable and hence produces strong spectral activity [61,62]. The experimental C-S stretch in **1** was observed at 815 cm^{-1} and the calculated B3LYP value appeared at 820 cm^{-1}. The C-N stretching in **2** was recorded at 1159 cm^{-1} with the computed value at 1186 cm^{-1} and, finally, the experimental C_2H_5 stretch in **3** appears at 2965 cm^{-1} which is the same as the calculated value.

3.3.3. C=O vibrations

The C=O bond in ketones is found in the region of 1680–1750 cm^{-1} [57,59]. The experimental bands of **1**–**3** were found to be in the range of 1645–1684 cm^{-1}. This downfield shift from the normal absorption of 1725 cm^{-1} is due to the presence of a high degree of conjugation of the carbonyl group with the olefinic bonds and aryl groups from both sides. The peaks observed at 1645, 1684 and 1645 cm^{-1} are for **1**, **2** and **3** respectively. The calculated C=O stretching vibrations for **1**, **2** and **3** appeared at 1649, 1641 and 1652 cm^{-1} respectively, as obtained with the B3LYP/6–311++G (d, p) level of theory.

3.3.4. C=C vibrations

The C=C stretching vibrations in alkenes and aromatic compounds normally occur in the regions of 1620–1680 cm^{-1} and 1400 - 1600 cm^{-1} respectively [57,59]. The experimental C=C stretching vibrations observed for **1** are at 1617 and 1586 cm^{-1} while the computed values occur at 1630 and 1598 cm^{-1} respectively. The experimental C=C stretching vibrations for **2** were recorded at 1630 and 1548 cm^{-1} and the calculated values fall at 1636 and 1600 cm^{-1} respectively, while, **3** has 1622 and 1588 cm^{-1} for the experimental C=C stretching vibrations with simulated C=C stretching vibrations at 1634 and 1592 cm^{-1} respectively. All the calculated results were in good agreement with the experimental data.

3.4. Electronic transitions

The nature of the electronic transitions in the observed UV–visible spectra of **1**–**3** and hydrogenated photoproducts of **1** and **3** have been studied by time-dependent density functional theory (TD-DFT). TD-DFT has emerged as a powerful tool for investigating the static and dynamic properties of molecules in their excited states, allowing for the best compromise between accuracy and

computational cost. The UV–vis spectra of the present compounds in vacuum as well as in various organic solvents (ethyl acetate, methanol and DMSO) were studied with TD-DFT at the B3LYP/6–311++G (d, p) level coupled with the Integral Equation Formalism Polarized Continuum Model (IEF-PCM), while the hydrogenated photoproducts were only studied in solvent phases. We give priority to these solvents because ethyl acetate is a less polar aprotic solvent, DMSO is a polar aprotic solvent, and methanol is a polar protic solvent acting as both hydrogen donor and acceptor. The greater the dielectric constant, the greater the polarity. These solvents cover a wide range of polarities and have different dielectric constants (ethyl acetate, $\varepsilon = 6.02$; methanol, $\varepsilon = 32.7$; and DMSO, $\varepsilon = 46.7$) [63–65]. The calculated absorption wavelengths (λ), oscillator strengths (*f*), dipole moments (μ), excitation energies (*E*) and excited lifetimes (τ) of **1**–**3** in vacuum and solution phases are displayed in Table 4. The τ of the compounds in both vacuum and different organic solvents were calculated from the relation, $\tau = \frac{1.499}{f(E)^2}$, where E (in cm^{-1}) is the energy gap between the ground state and first excited state, and *f* is the oscillator strength of the excited state [66–69].

It is observed that all the absorption bands in **1**–**3** and the hydrogenated photoproducts are red shifted in polar solvents (Figs. 4 and 5). Polar solvents are known to stabilize π* orbitals more than π orbitals [51]. This increase in stabilization of the excited states by polar solvents is the reason for the observed bathochromic shift of the absorption bands (Tables 4 and 5). The calculated electronic transitions are in good agreement with the experimental electronic transitions. The wavelength of maximum absorption, λ_{max}, is a function of substitution; the stronger the donor character of the substituent, the more electrons are pushed into the system, hence, the longer λ_{max}. The roles of the substituents and solvents influence the UV spectra of the present compounds. Evaluation of the TD-DFT calculations show that the significant transitions in compounds **1**–**3** are HOMO-1 to LUMO and HOMO to LUMO, and the most intense band in the compounds mainly originate due to HOMO → LUMO excitation. This may be due to the electronic transition of the carbonyl group; hence, electronic excitation is assigned to be n → π*. This transition originates from the lone pair on the central oxygen (n → π*) and is symmetry forbidden. The calculated UV absorption intensity is more intense in ethyl acetate, methanol and DMSO than in vacuum suggesting this is due to polarizability and the dielectric strength of the solvents.

To increase the band intensity or oscillator strength there should be a good overlap between the orbitals involved in the electronic transition. It could be observed that in a polar medium, the oscillator strengths are found to increase. This could be due to better orbital overlap. Thus, an increase in the polarity of the solvent increases the oscillator strengths and dipole interactions between solvent molecules and the solute thereby lowering the excitation energy (Table 4). Furthermore, the excited states lifetimes decrease with increase in polarity of the solvents. Therefore, solvent polarity decreases excitation energies and lifetime of the excited state of the present compounds (**1**–**3**) and increases their dipole moment.

It can be seen from Fig. 4, that absorption of **1**–**3** spans the entire UV region. UV radiation may be classified as UVC, UVB and UVA. As mentioned earlier, UVA and UVB can cause damage to the skin [70,71]. The absorption maxima of the studied molecules are found in the UVB and UVA regions. Thus, these molecules could have broad-spectrum UV-screening ability. However, when dilute solutions of compounds **1** and **3** were exposed to simulated solar radiation, they become photo-unstable (photodegraded) leading to a selective protonation of one of the olefinic bonds of the chromophore which is contrary to other reports [72,73]. Consequently, the formation of the hydrogenated photoproducts could be attributed to possible photolysis of the associated moisture, which invariably provided the protons for the hydrogenation of the olefinic bond [74]. Furthermore, the simulated results of the photoproducts are in good agreement with the experimental ones (Table 5). Compound **2** was found to be essentially photostable in the polar protic solvent methanol.

The analysis of the wavefunctions indicates that the electron absorptions of **1**–**3** correspond to the transition from the ground state to the first excited state ($S_0 \rightarrow S_1$) and is mainly described by a one-electron excitation from the HOMO to the LUMO.

3.5. Analysis of the frontier molecular orbitals

As known, molecular orbitals are obtained from the linear combination of the atomic orbitals of the atoms in a molecule and the most important orbitals are the HOMO and the LUMO, which are called frontier molecular orbitals, due to their localization at the outermost boundaries. The HOMO has a nucleophilic character since it can donate an electron, while the LUMO can be an electron

Table 4
Experimental (λ_{max}) and TD-DFT computed ($\lambda_{TD\text{-}DFT}$) wavelengths of maximum absorption, oscillator strengths (*f*), dipole moments (μ), excitation energies (E), and excited state lifetimes (τ) for **1**–**3** in vacuum and in different solvents.

Compounds	Solvent	λ_{max}/nm	$\lambda_{TD\text{-}DFT}$/nm	*f*	E/eV	μ/D	$\tau/10^{-5}$ ns
1	Vacuum	–	384	0.0645	3.2288	6.0785	3.4300
	Ethyl acetate	367	405	0.0949	3.0647	8.0705	2.5900
	Methanol	–	408	0.0951	3.0395	8.7378	2.6200
	DMSO	378	410	0.1001	3.025	8.7910	2.5200
2	Vacuum	–	386	0.0587	3.2138	5.6178	3.8000
	Ethyl acetate	369	417	0.0881	2.9748	7.9241	2.9600
	Methanol	386	423	0.0887	2.9308	8.7166	3.0500
	DMSO	386	425	0.0932	2.9141	8.7809	2.9100
3	Vacuum	–	338	0.0507	3.6662	3.6702	3.3800
	Ethyl acetate	329	351	0.0764	3.5354	4.9145	2.4100
	Methanol	339	352	0.0779	3.5191	5.3334	2.3900
	DMSO	338	354	0.0817	3.5056	5.3669	2.3000

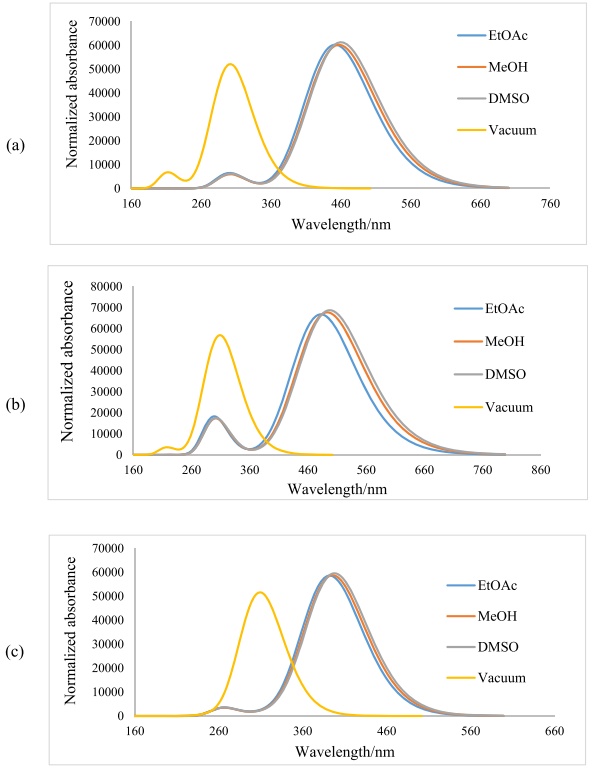

Fig. 4. TD-DFT absorbance spectra in various solvents for (a) **1**, (b) **2**, and (c) **3**.

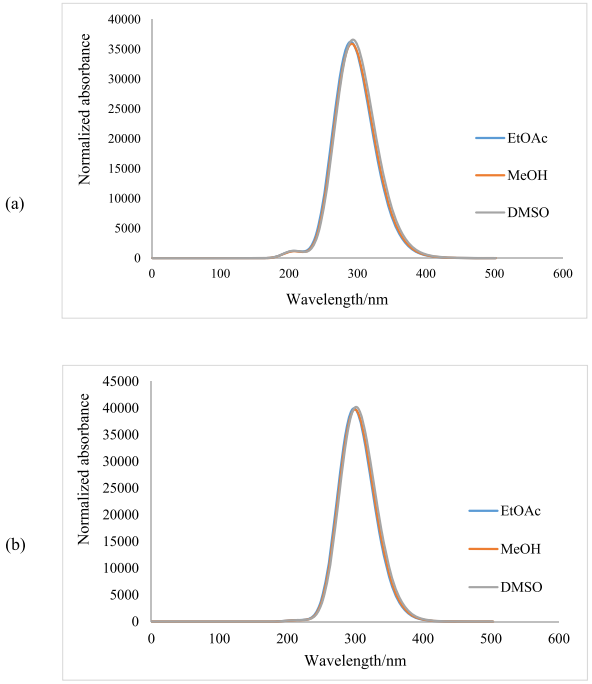

Fig. 5. TD-DFT absorption spectra of the hydrogenated photoproducts of (a) **1** and (b) **3** in various solvents.

Table 5
Experimental (λ_{max}) and TD-DFT computed ($\lambda_{TD\text{-}DFT}$) wavelengths of maximum absorption for the hydrogenated photoproducts of **1** and **3** in different solvents.

Photoproduct of compound	Solvents	λ_{max}/nm	$\lambda_{TD\text{-}DFT}$/nm
1	Ethyl acetate	311, 262	367, 276
	Methanol	NS	367, 273
	DMSO	323, 289, 265	369, 276, 273
3	Ethyl acetate	310, 266	316, 285
	Methanol	308, 261	317, 285
	DMSO	314	318, 287

NS – not soluble.

acceptor as it has an electrophilic character. Therefore, when an electron jumps from the HOMO to the LUMO, the electron density significantly decreases in the electron-donating moiety and is accompanied by an increase in the electron density of the electron-accepting moiety. The shapes of these molecular orbitals, their energies, as well as their energy gap, have many applications [75, 76]. HOMO-LUMO analysis plays an important role in determining the amount of energy required to add or remove electrons in a molecule. It also helps in predicting chemical reactivity, optical properties, as well as charge transfer properties of a molecule [53, 77–79].

The frontier molecular orbitals of **1**–**3** were obtained with the B3LYP method and the 6–311++G (d, p) basis set in vacuum and in various solvents for the optimized molecular structures. The Polarizable Continuum Model (PCM), together with the Integral Equation-Formalism Polarizable Continuum Model (IEF-PCM), was used to evaluate the solvent effect. Six important orbital energies of the molecules including the highest, second and third highest occupied molecular orbitals (HOMO, HOMO-1 and HOMO-2) and the lowest, second and third lowest unoccupied molecular orbitals (LUMO, LUMO+1 and LUMO+2) were calculated and are depicted in Supplementary Material Figs. S8–S10 and their energies are presented in Supplementary Material Table S1. The $\Delta E_{LUMO\text{-}HOMO}$ gap is commonly used as a stability index [80,81]; the higher the value the more stable the chemical system [82].

The ground state HOMO and LUMO distribution for **1**–**3** are shown in Fig. 6 and Supplementary Material Figs. S11 and S12. In these plots, the red and green colours represent the positive and negative phases of the molecular orbitals respectively. The HOMO and the LUMO energy eigenvalues and energy gaps in vacuum and various solvents are presented in Table 6. There is a remarkable difference in the energy gap computed in vacuum, ethyl acetate, methanol and DMSO (Table 6). For instance, the energy gaps of **1**–**3** in vacuum are higher than in all the solvents, revealing the role of solvent polarity in stabilizing the ground and excited states of the molecules.

The small $\Delta E_{HOMO\text{-}LUMO}$ values explain the eventual charge transfer interaction within **1**–**3** and the influence on their optical activities when they absorb UV light (Fig. 7). Obviously, the HOMOs of **1**–**3** represent a complete non-bonding (n-type) character because of the lone pair on their central oxygen. Specifically, the HOMO is localized over all atoms except the carbonyl atoms of the

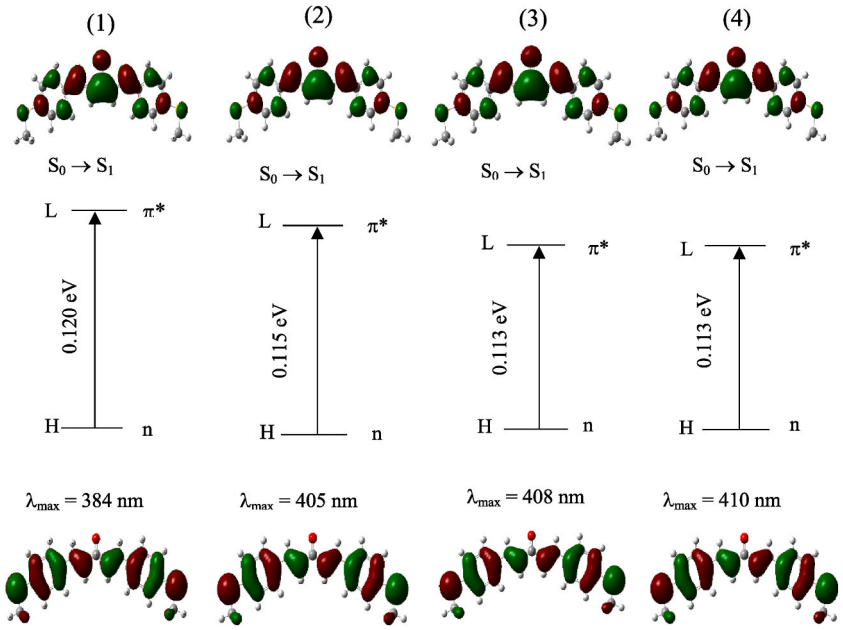

Fig. 6. Diagram of MOs involved in the electronic transition giving rise to the UV–vis absorption of **1** in (1) vacuum, (2) ethyl acetate, (3) methanol, and (4) DMSO obtained with the TD-DFT/B3LYP method and the 6-311G++ (d, p) basis set. The MOs depicted at the bottom and at the top are respectively the HOMO and LUMO.

Table 6
The energy eigenvalues of the frontier molecular orbitals ($\Delta E_{LUMO\text{-}HOMO}$) for **1**–**3** in vacuum and different solvents obtained at the B3LYP/6–311++G (d, p) level of theory.

Compound	Vacuum $\Delta E_{LUMO\text{-}HOMO}$/eV	Ethyl acetate $\Delta E_{LUMO\text{-}HOMO}$/eV	Methanol $\Delta E_{LUMO\text{-}HOMO}$/eV	DMSO $\Delta E_{LUMO\text{-}HOMO}$/eV
1	0.120	0.115	0.113	0.113
2	0.117	0.107	0.104	0.104
3	0.137	0.132	0.130	0.130

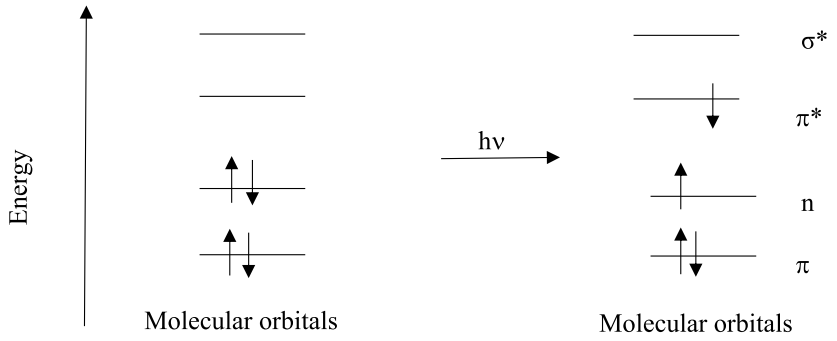

Fig. 7. Mechanism of UV light absorption for **1**–**3**.

compounds. The LUMO is dispersed over the whole molecule in both vacuum and solvents showing the π* character of the C=O bond. Hence, the transition $S_0 \rightarrow S_1$ is mainly due to the electronic transition from HOMO-LUMO (n - π*) (Fig. 7). It is interesting to note that the computational results were consistent with the experimental results where the loss of photo-absorption capacity of **1** and **3** in ethyl acetate, methanol and DMSO after the first 30 min of exposure to UV light was observed [20]. On the other hand, we did not observe any significant change in the photo-absorption capacity of **2** in methanol even after 4 h of irradiation; thus, **2** could be said to be photostable. However, a slight discrepancy exists between the experimental and computational results for the effects of methanol on the stability of **2**. This disagreement could be attributed to the limitation of the computational prediction. Therefore, we conclude that solvent polarity slightly enhances the probability of a transition for **1**–**3**.

3.6. DFT-based properties related to stability

The energies of the neutral, cationic and anionic species of **1**–**3** were calculated by natural population analysis by using the B3LYP/6–311++G (d, p) method and are presented in Supplementary Material Table S2. The understanding of the chemical reactivity of the compounds can be obtained from conceptual density functional theory (DFT) [83]. Global reactivity descriptors act as a bridge between the stability of the structures and global chemical reactivity [84]. The global reactivity descriptors give information about fundamental features of the chemical reactivity, such as ionization potential, electron affinity, global hardness and global softness, among others [85]. The energy values of the frontier molecular orbitals can be considered as a good starting point in order to determine these parameters. The difference between the HOMO-LUMO energy values is the most important determinant of chemical stability.

The hardness represents how a molecule resists deformation of its electron cloud during a chemical process, while its inverse is described as the global softness [86,87]. Hard systems have large energy gaps and are relatively small, stable, unreactive and not polarizable, while soft systems are large with small energy gaps and are highly polarizable and reactive as they easily interact [86–89]. Ionization potential is the minimum energy required in vacuum to remove an electron from an atom or molecule, while electron affinity describes the capability of an atom or molecule to attract electrons.

The calculated DFT-based quantities, such as electron affinity (E_A), ionization potential (IP), hardness (η), and softness (*S*), for **1**–**3** are presented in Table 7. It is clear from the results that **1**–**3** have a small $\Delta E_{LUMO\text{-}HOMO}$, implying that the present compounds are highly reactive and soft. The electron-releasing substituents attached to **1** and **3** reduced their stability. It is of interest to note that **2** appears to be more stable than **1** and **3** (Table 7), hence, this result supports the experimental findings. The global hardness of these compounds increases as the global softness is reduced (Table 7).

Table 7
DFT-based quantities for **1**–**3** obtained at the B3LYP/6311++G (d, p) level of theory.

Compounds	E_A/eV	IP/eV	η/eV	*S*/eV
1	−1.41	6.93	4.17	0.12
2	−0.87	6.24	3.55	0.14
3	−1.31	7.40	4.36	0.11

3.7. Natural bond orbital analysis

Charge transfer is one of the essential factors for understanding the stability of a molecule. This can be investigated from natural bond orbital (NBO) analysis [54] by monitoring the atom charges [55]. The natural atomic charge (NAC) plays an important role in applying quantum mechanical calculations to molecular systems, as the atomic charge affects the electronic structure, dipole moment, and other properties of the molecule [56]. In this work, we have investigated the effect of three different types of electron-releasing substituents (-SCH_3, -$N(CH_3)_2$ and -C_2H_5) on the stability of **1**–**3** (Supplementary Material Table S3). Substituents have a tremendous influence on the stability of these compounds. The atoms in all the molecules are categorized into three groups (substituent, phenyl rings, and chromophore) and the charges are given in Table 8. Charge transfer occurred within the compounds as the substituents have excess electrons. The electron-donor ability of the substituents attached to the phenyl rings plays a very important role on the structural and electronic properties of the molecules as they share their excess electrons with the π electrons in the phenyl rings. It is evident from Table 8, that all the electrons donated by the substituents in **1** and **3** were fully accommodated by the phenyl rings thereby making the systems extremely saturated (highly reactive). Thus, when the systems absorbed UV light, the excess electrons could no longer be accommodated by the compounds, and this resulted in the opening of one of the π-bonds of the chromophore for bonding with any available hydrogen in the solution (photodegradation). However, for **2**, the electron donor-acceptor ability of the substituent (dimethyl amino group) attached to the phenyl ring plays a crucial role on the structural stability of the compound. The symmetry of the entire system allows free movement of the excess electrons from the chromophore to the phenyl rings and to the substituent when it absorbs UV light during irradiation. This allows for electron delocalization upon absorption of UV radiation with minimal reaction occurring.

3.8. Analysis of NMR chemical shifts

NMR spectroscopy is a powerful spectroscopic technique used in identifying structural and functional characteristics of compounds in both solid and liquid states. The gauge invariance atomic orbital (GIAO) approach within DFT has become a standard tool for computing absolute chemical shifts (δ, ppm) relative to tetramethylsilane (TMS). GIAO NMR (^{1}H and ^{13}C) calculations have been performed at the B3LYP/6–311++G (d, p) level of theory in the solvent (chloroform) phase (using the IEF-PCM model) for all the present compounds. The experimental and theoretical ^{1}H and ^{13}C NMR chemical shifts are given in Table 9. The NMR signals for some nuclei normally appear at different chemical shift values as each nucleus in the compounds is chemically unlike to another due to different surrounding electrons [90–92]. The NMR signals for organic compounds relative to TMS normally fall in the region 0–10 ppm for ^{1}H NMR, and 0–220 ppm for ^{13}C NMR. In the present study, the chemical shift values of molecules **1**–**3** and the hydrogenated photoproducts of **1** and **3** are observed in the region of 1–8 ppm for the ^{1}H NMR spectra, and from 15 to 190 ppm for ^{13}C NMR of **1**–**3**. A high density of electrons delocalized over a nucleus leads to a low value of the chemical shift (upfield) due to the shielding effect, and less electron density on the nucleus gives high values of the chemical shift (downfield) due to a deshielding effect.

In ^{13}C NMR, the signals due to C12 in all the three compounds appeared at higher chemical shift values because they are connected to a highly electronegative oxygen atom (deshielding effect) [45]. In the ^{1}H NMR spectrum, the atoms H28 - H46 from the substituent group are observed at low values of the chemical shift due to the addition of electron density (shielding effect) and the environmental effect as all the hydrogen atoms of the substituents are located on the molecule periphery [93,94], while the atoms H7, H9, H21, H22, H24, H25, H39, H40, H47 and H48 are observed at large values because of removal of electron density (deshielding) in all three compounds. The H35 and H36 are also observed at large chemical shift values because they are in the vicinity of the electronegative oxygen atom (large negative charge). The computed chemical shifts are compared with the experimental values as shown in Table 9. However, one should be aware of the expected 0.1–0.5 ppm deviations of proton chemical shifts from experiment in GIAO NMR calculations [95–100] due to geometry and method of calculation. A good correlation between the experimental and calculated chemical shifts of **1**–**3** for the proton and carbon resonances were obtained (Supplementary Material Figs. S13 and S14).

Additionally, Table 10 presents a comparison of the calculated and experimental ^{1}H chemical (δ) shifts of the hydrogenated photoproducts in chloroform solvent, with TMS as reference. It could be seen experimentally, that the protons α and β to the carbonyl were observed in the region of 2–4 ppm, while the calculated values were obtained in the region of 2–3 ppm (Table 10). The computed chemical shifts of the photoproducts are in good agreement with the experiment, which indicates the suitability of the applied DFT method functional and the basis set.

4. Conclusions

Remarkably, for the first time the photochemical properties of **1**–**3** were computed by an *ab initio* method. The calculations allowed detailed assignment of the UV spectral features and predicted the n → π* nature of the lowest-lying singlet transitions both in vacuum and different solvents. Due to the solvent effect, the dipole moments of the compounds in ethyl acetate, methanol and DMSO are slightly larger than in vacuum, whereas, excitation energies decrease with increase in solvent polarity. Furthermore, the energy gap of HOMO-LUMO in solvents are smaller than in vacuum, hence, solvent polarity slightly enhances the probability of transitions of the present compounds. The movement of π electrons from donor to acceptor, i.e., intramolecular charge transfer, makes **1** and **3** more polarized and the low $\Delta E_{LUMO\text{-}HOMO}$ gap could be responsible for the high reactivity of these compounds, which supports our experimental findings. Thus, inspection of the active FMOs revealed the photodegradation trends of **1** and **3** under UV irradiation. However, introducing a -$N(CH_3)_2$ substituent to **2** at the *para*-position improves its photostability towards simulated UV radiation. Thus, molecule **2** proved to be effective under prolonged UV exposure, indicating its potential to absorb and provide efficient

Table 8
The NBO charges of **1**–**3** at the B3LYP/6–311++G (d, p) level of theory.

Compound	Substituent	Phenyl ring	Chromophore
1	0.448	−0.419	−0.029
2	−0.047	0.132	−0.084
3	0.078	−0.067	−0.013

Table 9
Experimental and theoretical ^{1}H and ^{13}C NMR chemical shifts (with respect to TMS) for **1**–**3**. The theoretical values were obtained by the DFT/B3LYP method. The experimental values are from Ref. [20].

Compound	Atom	δ_{Exp}/ppm	δ_{Theo}/ppm	Atom	δ_{Exp}/ppm	δ_{Theo}/ppm
1	H (28-34)	2.53	2.44	C (27, 31)	15.15	17.69
	H (25, 42)	7.04	7.12	C (1, 15)	124.54	125.54
	H (7, 21)	7.26	7.17	C (11, 13)	126.00	127.49
	H (39, 40)	7.54	7.47	C (2, 5, 14, 17)	128.75	130.43
	H (35, 36)	7.70	8.01	C (3, 19)	131.33	135.21
				C (4, 18)	142.30 142.63	138.64
				C (12)	188.69	189.89
2	H (35-46)	3.05	3.02	C (33, 34)	40.15	40.93
	H (21, 22)	6.71	6.67	C (5, 17)	111.91	113.89
	H (24, 25)	6.91	6.88	C (11, 13)	121.36	124.17
	H (47, 48)	7.53	7.48	C (3, 19)	122.97	127.31
	H (27, 28)	7.70	7.93	C (2, 14)	130.08	131.13
				C (4, 18)	142.94	140.49
				C (16, 23)	151.79	152.36
				C (12)	188.91	189.07
3	H (34-36)	1.28	1.28	C (31, 32)	15.32	10.39
	H (39-42)	2.71	2.95	C (29, 30)	28.86	30.11
	H (24, 25)	7.07	7.21	C (11, 13)	124.67	128.13
	H (7, 21)	7.27	7.48	C (1, 15)	128.51	129.17
	H (9, 22)	7.56	7.51	C (2, 14)	128.52	129.81
	H (28, 44)	7.74	7.82	C (5, 17)	132.38	134.83
				C (4, 18)	143.21	138.79
				C (10, 23)	147.26	150.56
				C (12)	189.11	190.35

Table 10
Experimental and theoretical ^{1}H NMR chemical shifts of the hydrogenated products of **1** and **3** (with respect to TMS). The theoretical values were obtained by the DFT/B3LYP method. Experimental values are from Ref. [20].

Photoproduct of compound	Atom	δ_{Exp}/ppm	δ_{Theo}/ppm
1	H (29-34)	2.48	2.41
	H (25, 26)	3.48	2.68
	H (21, 24)	3.73	2.76
	H (7, 18, 20)	6.61	6.86
	H (40, 42)	7.18	7.29
	H (39)	7.23	7.37
	H (37. 38)	7.31	7.52
	H (23)	7.77	7.89
3	H (29-34)	1.22	1.26
	H (24, 26, 43-46)	2.64	2.63
	H (21, 25)	3.77	2.77
	H (20)	6.63	6.97
	H (38)	7.15	7.25
	H (7, 36, 37, 40)	7.26	7.40
	H (18, 35)	7.60	7.55
	H (23)	7.80	7.96

protection against harmful UV radiation and overcome the photo-instability shortfall of current chemical UV filters. Hence, it can be treated as a promising candidate for UV filters in sunscreen formulations. Interestingly, for the first time the excited state lifetimes were calculated in vacuum and solvents. It was seen that solvent polarity significantly reduced the excited state lifetimes of the compounds. All theoretical results were compared with the experimental findings (UV–vis, FTIR and NMR spectra) and were found to be in good agreement. Thus, this work has shown that molecular modelling strategies can assist to rationalize experimental results. It has also shown that the dimethyl amino substituent allows for structural stability.

CRediT authorship contribution statement

Buhari Magaji: Writing – original draft, Methodology, Investigation. **Parvesh Singh:** Supervision, Conceptualization. **Adam A. Skelton:** Supervision. **Bice S. Martincigh:** Writing – review & editing, Supervision, Resources, Project administration, Methodology, Conceptualization.

Availability of data

All data associated with this article are available in the text and Supplementary Material.

Declaration of competing interest

The authors declare that they have no known competing financial interests or personal relationships that could have appeared to influence the work reported in this paper.

Acknowledgements

The authors are grateful to the University of KwaZulu-Natal, the CSIR National Laser Centre, and the National Research Foundation of South Africa, for providing research funding. BM thanks his employer, Gombe State University, for granting him leave to pursue his doctoral studies.

Appendix A. Supplementary data

Supplementary data to this article can be found online at https://doi.org/10.1016/j.heliyon.2024.e39910.

References

[1] M.S. Latha, J. Martis, V. Shobha, R.S. Shinde, S. Bangera, B. Krishnankutty, S. Bellary, S. Varughese, P. Rao, B.R. Naveen Kumar, Sunscreening agents: a review, J. Clin. Aesthet. Dermatol. 6 (2013) 16–26.
[2] H.V. DeBuys, S.B. Levy, J.C. Murray, D.L. Madey, S.R. Pinnel, Modern approaches to photoprotection, Dermatol. Clin. 18 (2000) 577–590.
[3] S. Lautenschlager, H.C. Wulf, M.R. Pittelkow, Photoprotection, Lancet. 370 (2007) 528–537.
[4] T. Matsunaga, K. Hieda, O. Nikaido, Wavelength dependent formation of thymine dimers and (6-4) photoproducts in DNA by monochromatic ultraviolet light ranging from 150 to 365 nm, Photochem. Photobiol. 54 (1991) 403–410.
[5] D. Moyal, Prevention of ultraviolet-induced skin pigmentation, Photodermatol. Photoimmunol. Photomed. 20 (2004) 243–247.
[6] A. Fourtanier, D. Moyal, S. Seite, UVA filters in sun-protection products: regulatory and biological aspects, Photochem. Photobiol. Sci. 11 (2012) 81–89.
[7] R.M. Lavker, D.A. Veres, C.J. Irwin, K.H. Kaidbey, Cumulative effects from repeated exposures to suberythemal doses of UVB and UVA in human skin, J. Am. Acad. Dermatol. 32 (1995) 53–62.
[8] P.E. Stoebner, R. Poosti, K. Djoukelfit, J. Martinez, L. Meunier, Decreased human epidermal antigen-presenting cell activity after ultraviolet A exposure: dose-response effects and protection by sunscreens *British J. Dermatol* 156 (2007) 1315–1320.
[9] H.V. DeBuys, S.B. Levy, J.C. Murray, D.L. Madey, S.R. Pinnell, Modern approaches to photoprotection, Dermatol. Clin. 18 (2000) 557–590.
[10] C.F. Garland, F.C. Garland, E.D. Gorham, Epidemiologic evidence for different roles of ultraviolet A and B radiation in melanoma mortality rates, Ann. Epidemiol. 13 (2003) 395–404.
[11] D. Lazovich, R.I. Vogel, M. Berwick, M.A. Weinstock, K.E. Anderson, E.M. Warshaw, Indoor tanning and risk of melanoma: a case-control study in a highly exposed population, Cancer Epidemiol. Biomarkers Prev. 19 (2010) 1557–1568.
[12] P.U. Giacomoni, Sunprotection: historical perspective, in: Shaath NA. Sunscreens (Ed.), Regulation and Commercial Development, Taylor & Francis Informa, Boca Raton, 2005, pp. 71–85, 3rd ed.
[13] P.C. Jou, R.J. Feldman, K.J. Tomecki, UV protection and sunscreens: what to tell patients, Cleve. Clin. J. Med. 79 (2012) 427–436.
[14] A. Fourtanier, D. Moyal, S. Seite, UVA filters in sun-protection products: regulatory and biological aspects, Photochem. Photobiol. Sci. 11 (2012) 81–89.
[15] M.E. Burnett, S.Q. Wang, Current sunscreen controversies: a critical review, Photodermatol. Photoimmunol. Photomed. 27 (2011) 58–67.
[16] F. Bruge, L. Tiano, P. Astolfi, M. Emanuelli, E. Damiani, Prevention of UVA-induced oxidative damage in human dermal fibroblasts by new UV filters, assessed using a novel *in vitro* experimental system, PLoS One 9 (2014) e83401.
[17] D. Dondi, A. Albini, N. Serpone, Interactions between different solar UVB/UVA filters contained in commercial suncreams and consequent loss of UV protection, Photochem. Photobiol. Sci. 5 (2006) 835–843.
[18] J. Kockler, M. Oelgemöller, S. Robertson, B.D. Glass, Photostability of sunscreens, J. Photochem. Photobiol., C 13 (2012) 91–110.
[19] G.J. Mturi, B.S. Martincigh, Photostability of the sunscreening agent 4-tert-butyl-4-methoxydibenzoylmethane (avobenzone) in solvents of different polarity and proticity, J. Photochem. Photobiol., A: Chemistry 200 (2008) 410–420.
[20] B. Magaji, P. Singh, A.A. Skelton, B.S. Martincigh, Synthesis, photostability and antibacterial activity of a series of symmetrical α,β-unsaturated ketones as potential UV filters, J. Photochem. Photobiol., A: Chemistry 445 (2023) 115018.
[21] L.L. Franco, M.V. de Almeida, L.F.R. E Silva, P.P.R. Vieira, A.M. Pohlit, M.S. Valle, Synthesis and antimalarial activity of dihydroperoxides and tetraoxanes conjugated with bis(benzyl)acetone derivatives, Chem. Biol. Drug Des. 79 (2012) 1–8.
[22] J.R. Dimmock, P. Kumar, A.J. Nazarali, N.L. Motaganahalli, T.P. Kowalchuk, M.A. Beazely, J.W. Quail, E.O. Oloo, T.M. Allen, J. Szydlowski, E. DeClercq, J. Balzarini, Cytotoxic 2,6-bis(arylidene)cyclohexanones and related compounds, Eur. J. Med. Chem. 35 (2000) 967–977.
[23] J.R. Dimmock, M.P. Padmanilayam, G.A. Zello, K.H. Nienaber, T.M. Allen, C.L. Santos, E. De Clercq, J. Balzarini, E.K. Manavathu, J.P. Stables, Cytotoxic analogues of 2,6-bis(arylidene)cyclohexanones, Eur. J. Med. Chem. 38 (2003) 169–177.
[24] W.M. Weber, L.A. Hunsaker, S.F. Abcouwer, L.M. Decka, D.L. Vander Jagt, Anti-oxidant activities of curcumin and related enones, Bioorg. Med. Chem. 13 (2005) 3811–3820.

[25] R. Costi, R. Di Santo, M. Artico, S. Massa, R. Ragno, R. Loddo, M. La Colla, E. Tramontano, P. La Collad, A. Panid, 2,6-bis(3,4,5-trihydroxybenzylydene) derivatives of cyclohexanone: novel potent HIV-1 integrase inhibitors that prevent HIV-1 multiplication in cell-based assays, Bioorg. Med. Chem. 12 (2004) 199–215.

[26] R.B. Aher, G. Wanare, N. Kawathekar, R.R. Kumar, N.K. Kaushik, D. Sahal, V.S. Chauhan, Dibenzylideneacetone analogues as novel *Plasmodium falciparum* inhibitors, Bioorg. Med. Chem. Lett. 21 (2011) 3034–3036.

[27] M.J. Frisch, G.W. Trucks, H.B. Schlegel, G.E. Scuseria, M.A. Robb, J.R. Cheeseman, G. Scalmani, V. Barone, B. Mennucci, G.A. Petersson, H. Nakatsuji, M. Caricato, X. Li, H.P. Hratchian, A.F. Izmaylov, J. Bloino, G. Zheng, J.L. Sonnenberg, M. Hada, M. Ehara, K. Toyota, R. Fukuda, J. Hasegawa, M. Ishida, T. Nakajima, Y. Honda, O. Kitao, H. Nakai, T. Vreven, J.A. Montgomery, J.E. Peralta, F. Ogliaro, M. Bearpark, J.J. Heyd, E. Brothers, K.N. Kudin, V. N. Staroverov, T. Keith, R. Kobayashi, J. Normand, K. Raghavachari, A. Rendell, J.C. Burant, S.S. Iyengar, J. Tomasi, M. Cossi, N. Rega, J.M. Millam, M. Klene, J.E. Knox, J.B. Cross, V. Bakken, C. Adamo, J. Jaramillo, R. Gomperts, R.E. Stratmann, O. Yazyev, A.J. Austin, R. Cammi, C. Pomelli, J.W. Ochterski, R. L. Martin, K. Morokuma, V.G. Zakrzewski, G.A. Voth, P. Salvador, J.J. Dannenberg, S. Dapprich, A.D. Daniels, O. Farkas, J.B. Foresman, J.V. Ortiz, J. Cioslowski, D.J. Fox, Gaussian 09, in: Revision D.01, Gaussian, Inc., Wallingford CT, USA, 2013.

[28] A.D. Becke, Density functional thermochemistry. III. The role of exact exchange, J. Chem. Phys. 98 (1993) 5648.

[29] C. Lee, W. Yang, R.G. Parr, Development of Colle-Salvetti correlation-energy formula into a functional of electron density, Phys. Rev. B Condens. Matter 37 (1988) 785–789.

[30] A.D. Becke, Density-functional exchange-energy approximation with correct asymptotic behavior, Phys. Rev. A 38 (1988) 3098–3100.

[31] P. Stephens, F. Devlin, C. Chabalowski, M.J. Frisch, Ab initio calculation of vibrational absorption and circular dichroism spectra using density functional force fields, J. Phys. Chem. 98 (1994) 11623–11627.

[32] T. Singh, H.G. Kruger, K. Bisetty, T.D. Power, Theoretical study on the formation of a pentacyclo-undecane cage lactam, Comp. Theoret. Chem. 986 (2012) 63–70.

[33] T. Ansbacher, H.K. Srivastava, J.M. Martin, A. Shurki, Can DFT methods correctly and efficiently predict the coordination number of copper(I) complexes? A case study, J. Comp. Chem. 31 (2010) 75–83.

[34] Y. Zhao, N. González-García, D.G. Truhlar, Benchmark database of barrier heights for heavy atom transfer, nucleophilic substitution, association, and unimolecular reactions and its use to test theoretical methods, J. Phys. Chem. A 109 (2005) 2012–2018.

[35] Y. Zhao, D.G. Truhlar, Density functionals with broad applicability in chemistry, Acc. Chem. Res. 41 (2008) 157–167.

[36] F. Jensen, Atomic orbital basis sets, WIREs Comput. Mol. Sci. 3 (2012) 273–295.

[37] J.G. Hill, Gaussian basis sets for molecular applications, Int. J. Quantum Chem. 113 (2013) 21–34.

[38] R. Dennington, T. Keith, J. Millam, Gauss View, Version 5, Semichem Inc., 2009. Shawnee Mission.

[39] A.P. Scott, L. Radom, Harmonic vibrational frequencies: an evaluation of Hartree-Fock, Moller-Plesset, quadric configuration interaction, density functional theory, and semiempirical scale factors, J. Phys. Chem. 100 (1996) 16502–16513.

[40] I.I.I.D.J. Russell, NIST Computational Chemistry Comparison and Benchmark Database, 2016. NIST Standard Reference Database Number 101 Release 18, October 2016, http://cccbdb.nist.gov/. (Accessed 2 April 2018).

[41] G. Scalmani, M.J. Frisch, B. Mennucci, J. Tomasi, R. Cammi, V. Barone, Geometries and properties of excited states in the gas phase and in solution: theory and application of a time-dependent density functional theory polarizable continuum model, J. Chem. Phys. 124 (2006) 94107–94122.

[42] R.E. Stratmann, G.E. Scuseria, M.J. Frisch, An efficient implementation of timedependent density-functional theory for the calculation of excitation energies of large molecules, J. Chem. Phys. 109 (1998) 8218–8224.

[43] M. Cossi, N. Rega, G. Scalmani, V. Barone, Energies, structures, and electronic properties of molecules in solution with the C-PCM solvation model, J. Comp. Chem. 24 (2003) 669–681.

[44] S. Miertus, E. Scrocco, J. Tomasi, Electrostatic interaction of a solute with a continuum. A direct utilization of *ab initio* molecular potentials for the prevision of solvent effects, Chem. Phys. Lett. 55 (1981) 117–129.

[45] U. Weber, H. Thiele, NMR-spectroscopy: Modern Spectral Analysis, John Wiley & Sons, New York, USA, 2008.

[46] K. Wolinski, J.F. Hilton, P. Pulay, Efficient implementation of the gauge-independent atomic orbital method for NMR chemical shift calculations, J. Am. Chem. Soc. 112 (1990) 8251–8260.

[47] J.R. Cheeseman, G.W. Trucks, T.A. Keith, M.J. Frisch, A Comparison of models for calculating nuclear magnetic resonance shielding tensors, J. Chem. Phys. 104 (1996) 5497–5509.

[48] W. Kohn, A.D. Becke, R.G. Parr, Density functional theory of electronic structure, J. Phys. Chem. 100 (1996) 12974–12980.

[49] P. Geerlings, F. De Proft, W. Langenaeker, Conceptual density functional theory, Chem. Rev. 103 (2003) 1793–1874.

[50] R.G. Parr, L.V. Szentpaly, S. Liu, Electrophilicity index, J. Am. Chem. Soc. 121 (1999) 1922–1924.

[51] P.K. Chattaraj, H. Lee, R.G. Parr, HSAB principle, J. Am. Chem. Soc. 113 (1991) 1855–1856.

[52] E. Frimpong, A.A. Skelton, B. Honarparvar, DFT study of the interaction between DOTA chelator and competitive alkali metal ions, J. Mol. Graphics and Model. 76 (2017) 70–76.

[53] F.Y. Adeowo, B. Honarparvar, A.A. Skelton, The interaction of NOTA as a bifunctional chelator with competitive alkali metal ions: a DFT study, RSC Adv. 6 (2016) 79485–79496.

[54] J. Foster, F. Weinhold, Natural hybrid orbitals, J. Am. Chem. Soc. 102 (1980) 7211–7218.

[55] V. Balachandran, K. Parimala, Tautomeric purine forms of 2-amino-6-chloropurine (N_9H_{10} and N_7H_{10}): structures, vibrational assignments, NBO analysis, hyperpolarizability, HOMO–LUMO study using B3 based density functional calculations, Spectrochim. Acta 96 (2012) 340–351.

[56] S. Sebastian, S. Sylvestre, J. Jayabharathi, S. Ayyapan, M. Amalanathan, K. Oudayakumar, I.A. Herman, Study on conformational stability, molecular structure, vibrational spectra, NBO, TD-DFT, HOMO and LUMO analysis of 3,5-dinitrosalicylic acid by DFT techniques, Spectrochim. Acta: Mol. Biomol. Spec. 136 (2015) 1107–1118.

[57] G. Socrates, Infrared Characteristic Group Frequencies, Wiley Interscience Publications, New York, USA, 1980.

[58] V.K. Rastogi, A.M. Palafox, R.P. Tanwar, L. Mittal, 3,5-Difluorobenzonitrile: *ab initio* calculations, FTIR and Raman spectra, Spectrochim. Acta, Part A 58 (2002) 1987–2004.

[59] R.M. Silverstein, B.G. Clayton, C.M. Terence, Spectrometric Identification of Organic Compounds, John Wiley & Sons Inc., New York, USA, 1981.

[60] J. Coates, Interpretation of Infrared Spectra, A Practical Approach, John Wiley & Sons Ltd, Chichester, 2000.

[61] A. Raj, K. Raju, H.T. Varghese, C.M. Granadeiro, H.I.S. Nogueira, C.Y. Panicker, IR, Raman and SERS spectra of 2-(methoxycarbonylmethylsulfanyl)-3,5-dinitrobenzene carboxylic acid, J. Braz. Chem. Soc. 20 (2009) 549–559.

[62] V. Arjunan, A. Raj, P. Ravindran, S. Mohan, Structure–activity relations of 2-(methylthio)benzimidazole by FTIR, FT-Raman, NMR, DFT and conceptual DFT methods, Spectrochim. Acta Part A: Mol. Biomol. Spect. 118 (2014) 951–965.

[63] R. Cammi, B. Mennucci, J. Tomasi, Fast evaluation of geometries and properties of excited molecules in solution: a Tamm–Dancoff model with application to 4-dimethylaminobenzonitrile, J. Phys. Chem. A 104 (2000) 5631–5637.

[64] M. Cossi, V. Barone, Solvent effect on vertical electronic transitions by the polarizable continuum model, J. Chem. Phys. 112 (2000) 2427–2435.

[65] M. Cossi, V. Barone, Time-dependent density functional theory for molecules in liquid solutions, J. Chem. Phys. 115 (2001) 4708, 4117.

[66] K.K. Rohatgi-Mukherjee, Fundamentals of Photochemistry, Wiley, New York, 1978.

[67] S. Saravanan, V. Balachandran, Quantum mechanical study and spectroscopic (FT-IR, FT-Raman, UV–Visible) study, potential energy surface scan, Fukui function analysis and HOMO–LUMO analysis of 3-tert-butyl-4-methoxyphenol by DFT, Spectrochimic. Acta A 130 (2014) 604–620.

[68] Z. Asadi, M.B. Asnaashariisfahani, E. Vessally, M.D. Esrafili, Experimental and theoretical study on diethyl-(Z)-2-(5,7-diphenyl-1,3,4-oxadiazepin-2-yl)-2-butenedioate using different levels of computational methods, Spectrochim. Acta: Mol. Biomol. Spect. 140 (2015) 585–599.

[69] T.H. Wang, H.Y. Chu, I.T. Wang, Structures, molecular orbitals and UV–vis spectra investigations on methyl 1-benzyl-1H-1,2,3-triazole-4-carboxylate: a computational study, Spectrochim. Acta: Mol. Biomol. Spec. 131 (2014) 268–273.

[70] L.P. da Silva, P.J.O. Ferreira, M.S. Miranda, J.C.G. Esteves da Silva, A theoretical study of the UV absorption of 4-methylbenzylidene camphor: from the UVB to the UVA region, Photochem. Photobiol. Sci. 14 (2015) 465–472.
[71] R.K. Chaudhuri, M.A. Ollengo, P. Singh, B.S. Martincigh, 3-(3,4,5-Trimethoxybenzylidene)-2,4-pentanedione: design of a novel photostabilizer with *in vivo* SPF boosting properties and its use in developing broad-spectrum sunscreen formulations, Int. J. Cosmet. Sci. 39 (2017) 25–35.
[72] G.N. Rao, C. Jonardhana, V. Ramanathan, T. Rajesh, H. Kumar, A convenient exercise in [2+2] cycloaddition using chemical ionization mass spectrometry, J. Chem. Educ. 83 (2006) 1667–1669.
[73] A. Schwarzer, E. Weber, Photochemical dimerization of a fluorinated dibenzylideneacetone in chloroform solution, Acta Cryst C70 (2014) 202–206.
[74] C.S. Liu, K. Shih, C.X. Sun, F. Wang, Oxidative degradation of propachlor by ferrous and copper ion activated persulfate, Sci. Total Env. 416 (2012) 507–512.
[75] K. Fukui, T. Yonezawa, H.J. Shingu, A molecular-orbital theory of reactivity in aromatic hydrocarbons, J. Chem. Phys. 20 (1952) 722–725.
[76] L. Padmaja, C. Ravikumar, D. Sajan, I.H. Joe, V.S. Jayakumar, G.R. Pettit, F.O. Neilsen, Density functional study on the structural conformations and intramolecular charge transfer from the vibrational spectra of the anticancer drug combretastatin-A2, J. Raman Spectrosc. 40 (2009) 419–428.
[77] Y. Erdogdu, Investigations of FT-IR, FT-Raman, FT-NMR spectra and quantum chemical computations of esculetin molecule, Spectrochim. Acta 106 (2013) 25–33.
[78] O. Dereli, Molecular structure and spectral (FT-IR, Raman) investigations of 3-aminocoumarin, Opt. Spectrsc. 120 (2016) 690–700.
[79] Z. Demircioglu, C. Albayrak, O. Büyükgüngör, Experimental (X-ray, FT-IR and UV–vis spectra) and theoretical methods (DFT study) of (*E*)-3-methoxy-2-[(*p*-tolylimino)methyl]phenol, Spectrochim. Acta: Mol. Biomol. Spect. 128 (2014) 748–758.
[80] D. Lewis, C. Ioannides, D.V. Parke, Interaction of a series of nitriles with the alcohol-inducible isoform of P450: computer analysis of structure-activity relationships, Xenobiotic 24 (1994) 401–408.
[81] S.B. Vepuri, H.C. Devarajegowda, M.E. Soliman, Synthesis, characterization and molecular modelling of a novel dipyridamole supramolecule X-ray structure, quantum mechanics and molecular dynamics study to comprehend the hydrogen bond structure activity relationship, J. Mol. Struct. 1105 (2016) 194–204.
[82] Z. Zhou, R.G. Parr, Activation hardness: new index for describing the orientation of electrophilic aromatic substitution, J. Am. Chem. Soc. 112 (1990) 5720–5724.
[83] R.G. Parr, W. Yang, Density Functional Theory of Atoms and Molecules, University Press, Oxford, 1989.
[84] R. Vijayaraj, V. Subramanian, P.K. Chattaraj, Comparison of global reactivity descriptors calculated using various density functionals: a QSAR perspective, J. Chem. Theory Comput. 5 (2009) 2744–2753.
[85] J. Padmanabhan, R. Parthasarathi, M. Elango, V. Subramanian, B.S. Krishnamoorthy, S. Gutierrez-Oliva, A. Toro-Labbe, D.R. Roy, P.K. Chattaraj, Multiphilic descriptor for chemical reactivity and selectivity, J. Phys. Chem. A 111 (2007) 9130–9138.
[86] Z.M. Kotena, R. Behjatmanesh-Ardakani, R. Hashim, V.M. Achari, Hydrogen bonds in galactopyranoside and glucopyranoside: a density functional theory study, J. Mol. Model. 19 (2013) 589–599.
[87] H.F. Hizaddin, R. Anantharaj, M.A. Hashim, A quantum chemical study on the molecular interaction between pyrrole and ionic liquids, J. Mol. Liq. 194 (2014) 20–29.
[88] G. Zhang, C.B. Musgrave, Comparison of DFT methods for molecular orbital eigenvalue calculations, J. Phys. Chem. A 111 (2007) 1554–1561.
[89] M.A. Amin, O. Hazzazi, F. Kandemirli, M. Saracoglu, Inhibition performance and adsorptive behavior of three amino acids on cold-rolled steel in 1.0 M HCl-chemical, electrochemical, and morphological studies, Corr 68 (2012) 688–698.
[90] M. Alam, D.U. Lee, Synthesis, spectroscopic and computational studies of 2-(thiophen-2-yl)-2,3-dihydro-1H-perimidine: an enzymes inhibition study, Comp. Biol. Chem. 64 (2016) 185–201.
[91] M. Alam, M.J. Alam, A.A. Shahab, S.A.A. Nami, M.S. Khan, S. Ahmad, D.U. Lee, DFT, Hirshfeld surfaces, spectral and *in vivo* cytotoxic studies of 7a-aza-B-homostigmast-5-eno [7a,7-d] tetrazole, J. Mol. Struct. 1099 (2015) 588–600.
[92] S.A.A. Nami, N. Sarikavakli, M.J. Alam, M. Alam, S. Park, S. Ahmad, Detailed molecular, structural and spectral studies of bimetallic salt [Ni(L)][$CoCl_4$] where L 1/4 3,7-bis(2-aminoethyl)-1,3,5,7- tetraazabicyclo(3.3.1)nonane, J. Mol. Struct. 1138 (2017) 90–101.
[93] M. Steglich, C. Jager, F. Huisken, M. Friedrich, W. Plass, H.J. Rader, K. Mullen, T. Henning, The abundance of hydrocarbon functional groups in the interstellar medium infra red from laboratory spectra of hydrogenated and methylated polycyclic aromatatoc hydrocarbon, Astrophys. J. Suppl. Ser. 208 (2013) 24–47.
[94] A. Srivastava, R. Mishra, S. Kumar, K. Dev, P. Tandon, R. Maurya, Molecular structure, spectral investigation (^{1}H NMR, ^{13}C NMR, UV-Visible, FT-IR, FT-Raman), NBO, intramolecular hydrogen bonding, chemical reactivity and first hyperpolarizability analysis of formononetin [7-hydroxy-3(4-methoxyphenyl) chromone]: a quantum chemical study, J. Mol. Struct. 1084 (2015) 55–73.
[95] J. Gauss, J.F. Stanton, Gauge-invariant calculation of nuclear magnetic shielding constants at the coupled–cluster singles and doubles level, J. Chem. Phys. 102 (1995) 251–253.
[96] J. Gauss, Analytic second derivatives for the full coupled-cluster singles, doubles, and triples model: nuclear magnetic shielding constants for BH, HF, CO, N_2 , N_2O, and O_3, J. Chem. Phys. 116 (2002) 4773–4776.
[97] T. Kupka, B. Ruscic, R.E. Botto, Toward Hartree-Fock- and density functional complete basis-set predicted NMR parameters, J. Phys. Chem. A 106 (2002) 10396–10407.
[98] T. Kupka, C. Lim, Polarization-consistent *versus* correlation-consistent basis sets in predicting molecular and spectroscopic properties, J. Phys. Chem. A 111 (2007) 1927–1932.
[99] K. Ruud, P.O. Astrand, P.R. Taylor, Zero-point vibrational effects on proton shieldings: functional-group contributions from *ab initio* calculations, J. Am. Chem. Soc. 123 (2001) 4826–4833.
[100] J.B. Foresman, A. Frisch, Exploring Chemistry with Electronic Structure Methods, Gaussian, Inc., Pittsburg, PA, 1996.